



Synthesis and visible light catalytic activity of HC/BiOCl/BiOBr microspheres

Xinyu Liu^{1,2} · Yuwei Zhu¹ · Shuang Gao¹ · Yulan Ren^{1,2}

Received: 7 June 2024 / Accepted: 28 August 2024

© The Author(s), under exclusive licence to Springer-Verlag GmbH Germany, part of Springer Nature 2024

Abstract

In this paper, waste peanut shell is used as raw material to produce biochar (HC), which makes reasonable use of agricultural waste and conforms to the concept of low carbon and environmental protection. HC/BiOCl/BiOBr microspheres are synthesized by solvothermal method. The crystal structure, morphology and optical properties of HC/BiOCl/BiOBr were characterized by XRD, SEM, TEM, EDX, XPS, PL and UV-Vis DRS. SEM shows that HC/BiOCl/BiOBr is composed of a spherical structure made of stacked sheets. The prepared HC/BiOCl/BiOBr showed high photocatalytic performance, and the degradation efficiency of RhB was 98.72% after 20 min of sunlight irradiation, which is higher than that of pure BiOCl and BiOBr. PL, EIS, BET and DRS spectra show that HC/BiOCl/BiOBr has low electron hole recombination, high photogenerated carrier separation rate, suitable aperture and strong visible light absorption capacity, which are the main reasons for its good photocatalytic activity. Free radical trapping experiments show that h^+ plays an important role in photocatalysis. The possible photocatalytic reaction mechanism of RhB degradation by HC/BiOCl/BiOBr was deduced. This study provides a new reference for the design of high performance and environmentally friendly photocatalytic materials.

Keywords Solvothermal · Biochar · BiOBr · BiOCl · Photocatalytic

1 Introduction

With the acceleration of urbanization and industrialization, the problem of environmental pollution is becoming more and more serious, among which the organic pollutants in industrial wastewater seriously threaten human health [1]. In recent years, the country has put forward the concept of green development, and more and more scholars have paid attention to environmental governance. Therefore, it is a very urgent task to find efficient and clean sewage treatment methods. At present, photocatalysis technology is considered as a promising wastewater treatment technology

because of its complete degradation, recycling and low energy consumption [2–4].

Among semiconductor photocatalysts, BiOCl has been widely studied due to its unique structure, but the band gap (E_g) of BiOCl is about 3.1–3.6 eV [5]. Due to the large band gap, it can only be excited by ultraviolet light, and the utilization rate of visible light is low, which greatly limits the practical application of BiOCl. Cen et al. [6] prepared $Ag_2WO_4/BiOCl$ composite photocatalyst by co-precipitation method for the degradation of RhB solution. $Ag_2WO_4/BiOCl$ composite photocatalyst showed higher photocatalytic performance than BiOCl, and the removal rate of RhB was 81.3% after sunlight irradiation for 25 min. Xu et al. [7] synthesized $BiOCl/g-C_3N_4$ composite material by hydrothermal method. After irradiation by 500 W xenon lamp for 180 min, the degradation efficiency of metronidazole (MZ) was 95%. Therefore, it is feasible to enhance the visible light catalytic activity of BiOCl by semiconductor composite method.

BiOBr has the advantages of narrow band gap (~2.8 eV) and stable chemical properties [8, 9]. Coupling wideband gap semiconductors with BiOBr to construct heterojunction photocatalysts is an effective and feasible method to

✉ Yulan Ren
rylmsy@163.com

¹ College of Chemistry and Chemical Engineering, Mudanjiang Normal University, Mudanjiang, Heilongjiang 157011, China

² Heilongjiang Province Key Laboratory of Photoelectric Functional Materials, Mudanjiang, Heilongjiang 157011, China

improve photocatalytic activity [10]. Liu et al. [11] successfully prepared HC/BiOBr/Bi₂WO₆ composite material by solvothermal method. Compared with BiOBr and Bi₂WO₆, HC/BiOBr/Bi₂WO₆ has higher photocatalytic activity, and the degradation efficiency of RhB is 98.91% after 180 min irradiation by 7 W LED lamp. Ma et al. [12] synthesized ZnO/BiOBr heterojunctions by precipitation-hydrothermal method. The formation of ZnO/BiOBr heterojunctions is conducive to the efficient separation and migration of e⁻-h⁺ pairs, and the degradation efficiency of tetracycline by composite photocatalyst is significantly higher than that of pure ZnO.

Biochar is a conductive carbon material developed in recent years, which has the advantages of abundant functional groups, large surface area, large pore volume, simple preparation process and low cost and has been used in the study of photocatalysts [13, 14]. Fan et al. [15] synthesized HC/BiVO₄ composite photocatalyst using glucose as carbon source by one-step hydrothermal method. After 300 W xenon lamp irradiation for 120 min, the degradation efficiency of tetracycline reached 86.4%. The results show that the combination of biochar and some bismuth photocatalysts can provide more adsorption sites for organic dye pollutants, promote photocharge transfer, inhibit the photo-carrier recombination, and effectively remove organic dye pollutants. At the same time, biochar uses waste crops as raw materials, which can reduce environmental pollution caused by the incineration of waste crops such as peanut shells and realize waste utilization.

In our previous work, HC/BiOCl composite photocatalysts were synthesized by solvothermal method [16]. HC/BiOCl has good degradation ability for RhB because of its has a high photogenic carrier separation rate. In this paper, semiconductor composite is carried out on the basis of previous work. HC/BiOCl/BiOBr composite photocatalysts with high visible light catalytic activity were synthesized by one-step solvothermal method. HC/BiOCl/BiOBr has stronger photocatalytic performance than HC/BiOCl, which may be related to broadening the light absorption range of the sample.

2 Materials and methods

2.1 Preparation of biochar

The peanut shells were washed and dried, crushed and passed through a 40-mesh sieve. Under magnetic stirring, 0.5 g peanut shell powder was added to 20 mL glycol, mixed evenly, and hydrothermal reaction was performed at 180 °C for 12 h. The product was washed with distilled water and anhydrous ethanol, dried at 70°C and recorded as HC.

2.2 Preparation of HC/BiOCl/BiOBr

Weigh 1 mmol Bi(NO₃)₃·5H₂O and dissolve in 30 mL glycol. Under magnetic stirring, 0.5 mmol KCl, 0.5 mmol KBr, 0.1 g PVP and 0.01 g HC are added successively. After stirring well, transfer to a high-pressure reactor and heat at 120 °C for 12 h. After cooling, wash with anhydrous ethanol and distilled water for 3 times, and dry at 70 °C.

Under the optimal reaction conditions, no HC was added to synthesize BiOCl/BiOBr, no HC and KBr were added to synthesize BiOCl monomer, and no HC and KCl were added to synthesize BiOBr monomer.

2.3 Characterization

The crystalline phase and structure was identified by X-ray diffraction (XRD: Pannalytical B.V.) with Cu-K α radiation ($\lambda=0.154$ nm, 40 kV). Scanning electron microscopy (SEM: Hitachi S-4800) and transmission electron microscopy (TEM: JEM-ARM200F) were used to analyze the morphology and structure of samples. X-ray photoelectron spectroscopy (XPS: ESCALAB 250Xi) analyzed the surface properties of the samples. Photoluminescence spectra (PL) were characterized by fluorescence spectrophotometer (F-7000) (excitation wavelength: 297 nm). The Ultraviolet-visible diffuse reflectance spectra of different samples were measured by the Shimadzu UV-2600 spectrophotometer (200–800 nm), BaSO₄ was used as the reference substance. The specific surface area, pore volume and mean pore diameter of the material were measured by the 3 H-200PS2 specific surface area and pore diameter analyzer.

2.4 Photocatalytic test

Rhodamine B (RhB) was used as a simulated pollutant to test the photocatalytic activity of the prepared materials. First, 50 mg of sample and 100 mL of RhB solution (15 mg·L⁻¹) were added to a beaker. The solution was magnetically stirred in the dark for 30 min to reach the adsorption-desorption equilibrium. Turned on the 70 W metal halide lamp, 4 mL suspension was taken every 10 min, the supernatant was centrifugally taken and its absorbance was measured at the maximum absorption wavelength of 554 nm.

3 Results and discussions

3.1 Structure and morphology analysis

XRD were employed to analyze the crystalline structure and composition of sample. It can be seen from the XRD curve of HC that the wide peak at 22.4° corresponds to peak C

[17]. As can be seen from the Fig 1, the XRD curves of synthesized BiOCl and BiOBr are consistent with the information of the tetragonal BiOCl (PDF#06-0249) and the tetrahedral BiOBr (PDF#78-0348), respectively. Since BiOCl and BiOBr both belong to bismuth halide photocatalytic materials, the positions of diffraction peaks of BiOCl and BiOBr are relatively close [18]. After composite, it is found that the positions of all diffraction peaks of HC/BiOCl/BiOBr and BiOCl/BiOBr are between the corresponding diffraction peaks of BiOCl and BiOBr. The characteristic diffraction peaks of HC were not found in the XRD curve of HC/BiOCl/BiOBr composites, which may be due to the low content of HC in the composite photocatalyst [19].

SEM was used to examine the morphology of the fabricated photocatalysts. From Fig. 2 (a), it can be seen HC is an irregular sheet-like structure. As shown in Fig. 2 (b) and (c), both BiOBr and BiOCl consist of many small irregular

sheets. Among them, the BiOBr has a spherical structure with a particle size between 2 and 3 μm . And the BiOCl/BiOBr composite exhibits flowerlike structure (Fig. 2 (d)). When HC is added, the prepared HC/BiOCl/BiOBr composite is a sphere composed of tightly stacked sheets, which results in a large number of pores on the surface of the microspheres (Fig. 2 (e)). As shown in Fig. 3, EDX images confirmed the presence of Bi, Br, Cl, O and C in the ternary composite, and their distribution was relatively uniform.

In order to further confirm the microstructure of HC/BiOCl/BiOBr, TEM and HRTEM characterization were performed. Figure 4 (b) shows the lattice fringes with crystal plane spacing $d=0.1833$ and 0.1907 nm in the figure are consistent with the (1 1 3) crystal face of the tetragonal BiOCl and the (2 0 1) crystal face of the orthographic BiOBr, respectively. The results show that the HC/BiOCl/BiOBr composite has been successfully prepared.

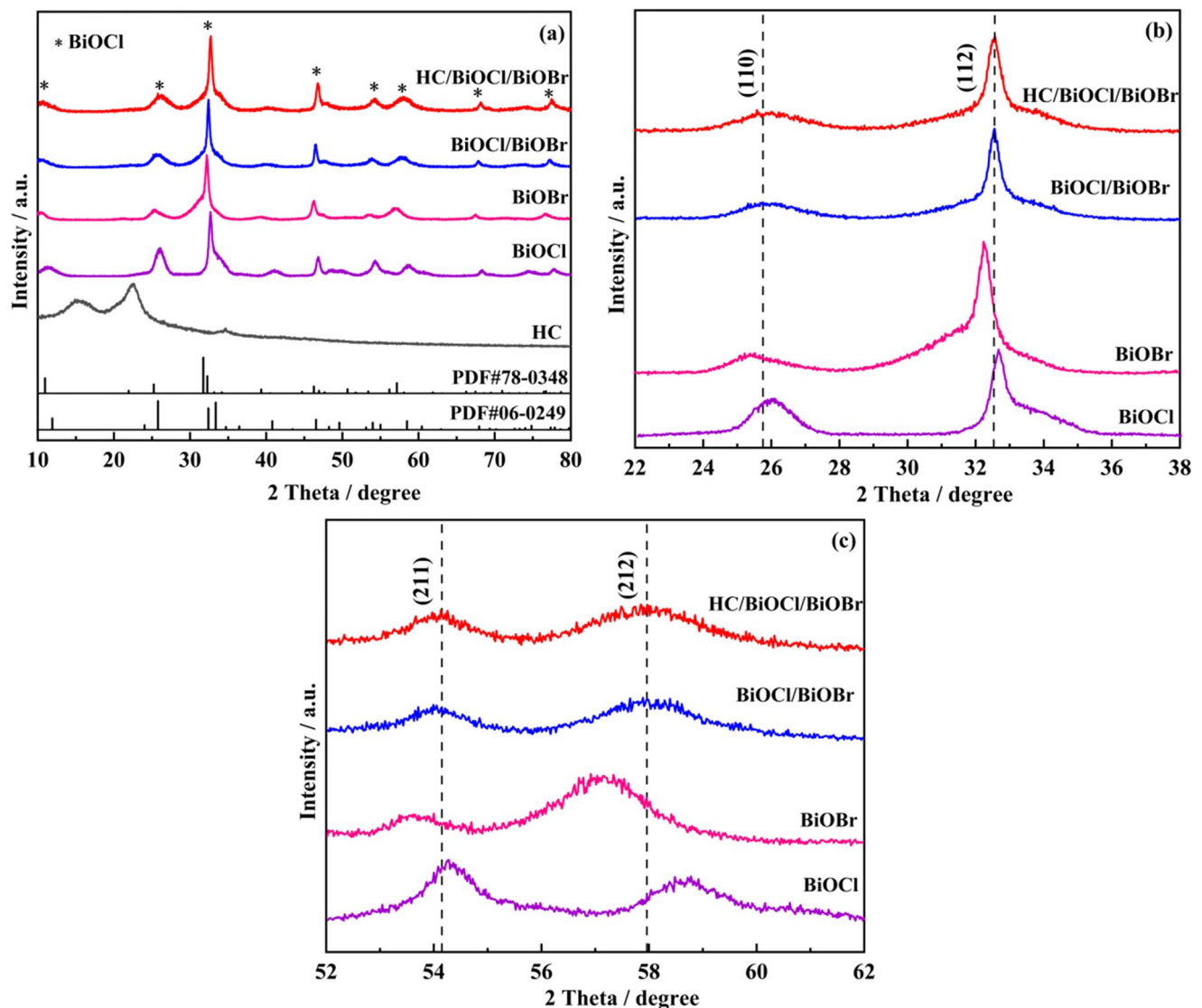


Fig. 1 The XRD pattern of samples

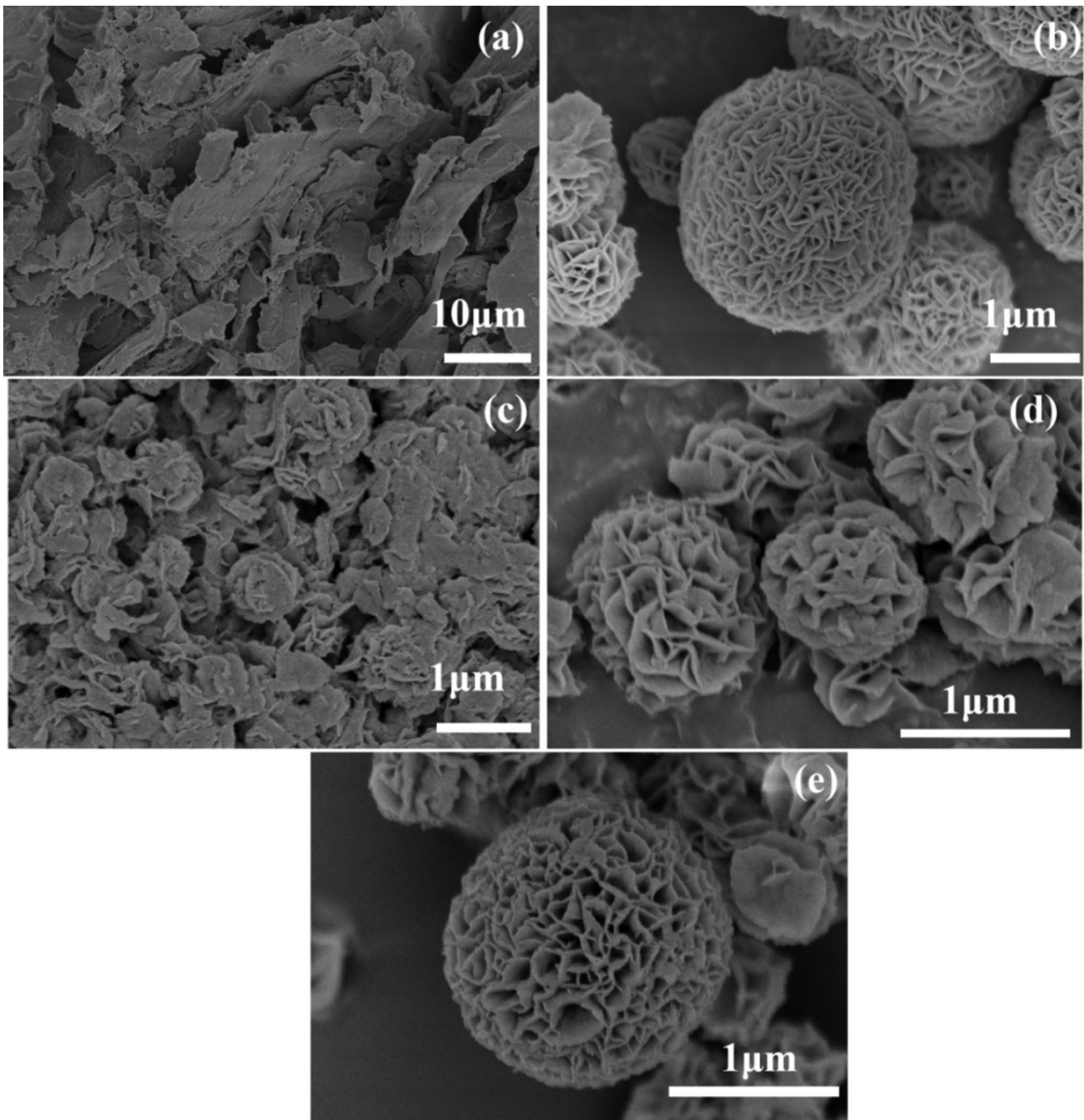


Fig. 2 SEM images of the samples: HC (a), BiOBr (b), BiOCl (c), BiOCl/BiOBr (d), HC/BiOCl/BiOBr (e)

Figure 5 demonstrates the XPS spectra of HC/BiOCl/BiOBr. In Fig. 5 (a), Bi, Cl, Br, O and C elements are present in ternary composite. Figure 5 (b) shows two peaks at 164.10 eV and 158.80 eV, which belong to Bi $4f_{5/2}$ and Bi $4f_{7/2}$, indicating that the chemical valence state of bismuth in HC/BiOCl/BiOBr composite is +3 valence [20]. In Fig. 5 (c), there are two distinct peaks at 199.20 eV and 197.60 eV, corresponding to Cl $2p_{1/2}$ and Cl $2p_{3/2}$, respectively [21]. In Fig. 5 (d), the peaks at 68.76 eV and 69.81 eV

correspond to Br $3d_{5/2}$ and Br $3d_{3/2}$ in BiOBr [22]. As shown in Fig. 5 (e), the XPS spectrum of O 1s can be fitted with three characteristic peaks. The peak at 529.66 eV is attributed to lattice oxygen in the sample, the peak at 531.03 eV is attributed to the adsorbed oxygen or C-O bond on the corresponding sample surface, and the peak at 532.46 eV is attributed to the oxygen vacancy or C=O bond in the sample [23]. Figure 5 (f) shows the XPS spectrum of C 1s. After fitting, five characteristic peaks can be observed. The

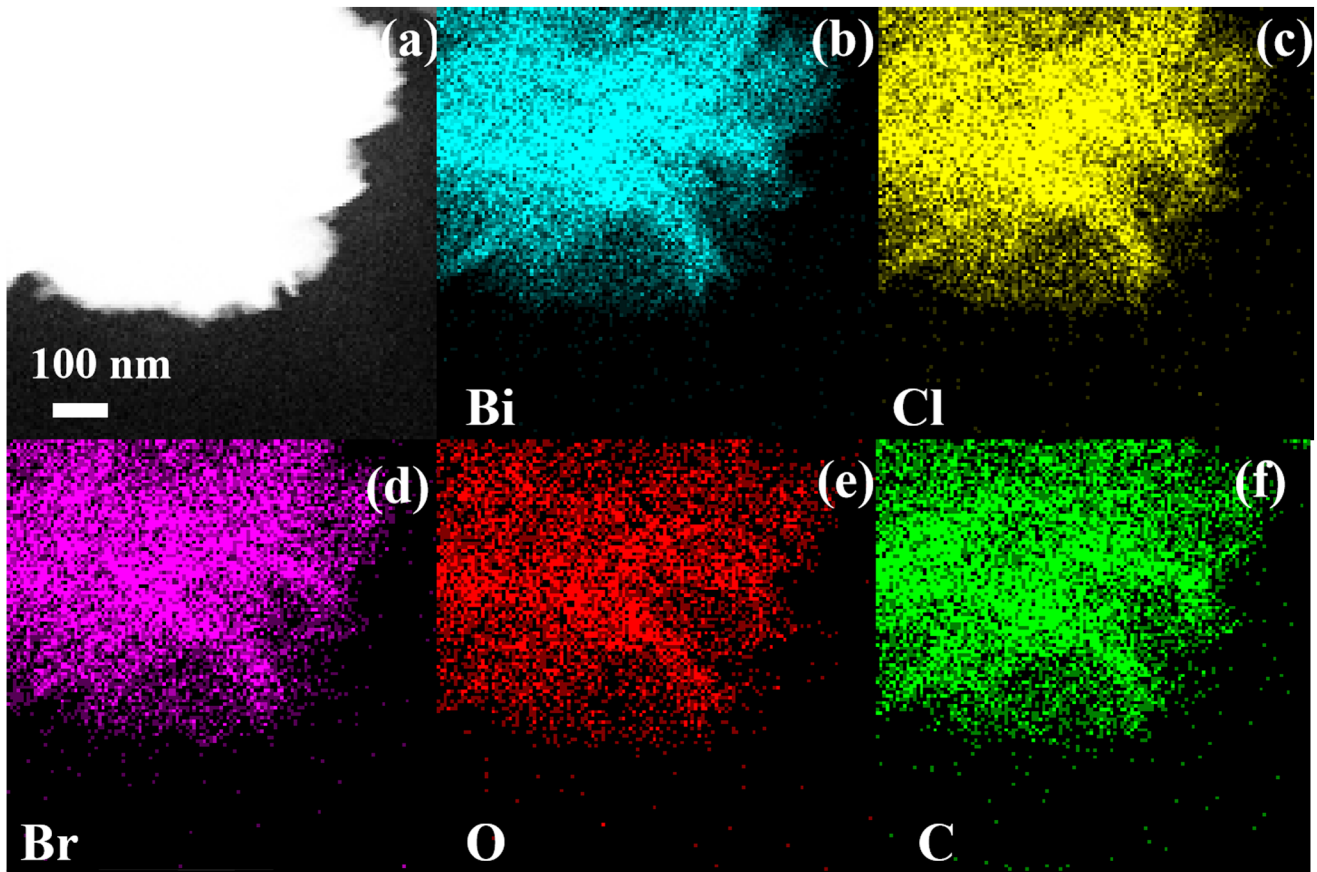


Fig. 3 The EDX images of HC/BiOCl/BiOBr

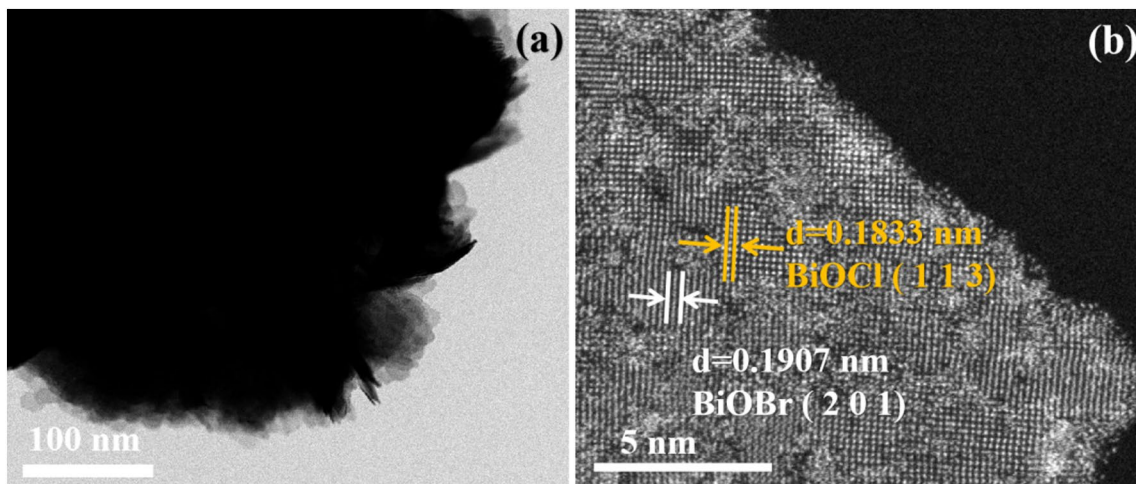


Fig. 4 The TEM and HRTEM images of HC/BiOCl/BiOBr

peak at 284.23 eV belongs to the C=C bond in the sample, the peak at 284.80 eV belongs to the C-C bond, the peak at 285.71 eV belongs to the C-O bond in the sample, and the peak at 287.21 eV corresponds to the C=O bond in the sample. The peak at 288.07 eV corresponds to the O-C=O bond in the sample [24, 25]. XPS spectra show that the HC/

BiOCl/BiOBr composites have been successfully synthesized, which is consistent with XRD and HRTEM analysis results.

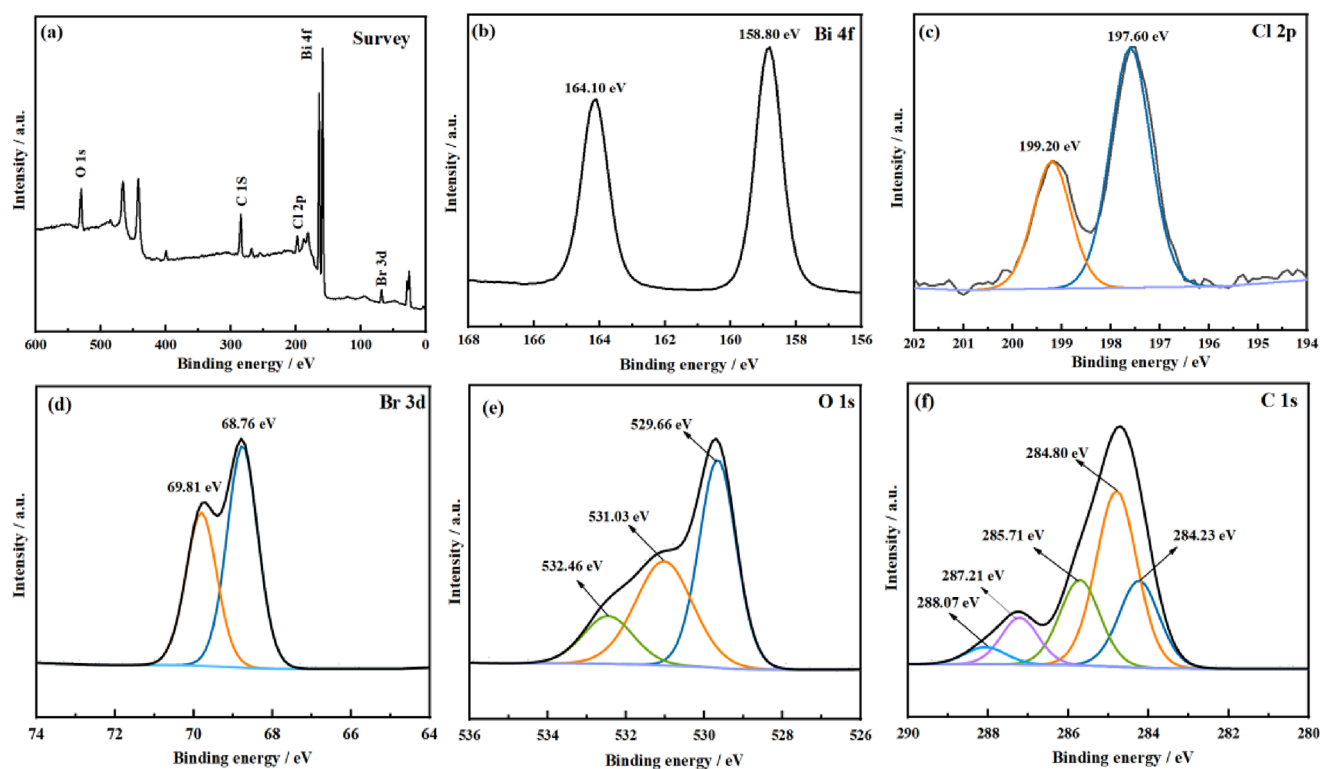


Fig. 5 XPS spectra of HC/BiOCl/BiOBr

3.2 Photocatalytic activity analysis

The photocatalytic activity of samples can be evaluated by degrading 15 mg/L RhB, as shown in Fig. 6 (a). RhB does not degrade in the absence of a photocatalyst or light irradiation. BiOCl, BiOBr and BiOCl/BiOBr exhibit poor catalytic activity, and the degradation efficiency was only 54.86%, 64.65% and 73.23% after 30 min irradiation with 70 W-metal halide lamp. In contrast, HC/BiOCl/BiOBr showed excellent photocatalytic performance, with a degradation efficiency of 99.41% within 30 min. Fig 6 (b) shows that HC/BiOCl/BiOBr had the highest rate constant K value of 0.16612 min^{-1} , which was greater than that of 0.03834 min^{-1} for HC/BiOCl, and was 6.46, 4.96 and 3.64 times higher than that of BiOCl, BiOBr and BiOCl/BiOBr, respectively.

In order to investigate the application range of photocatalysts, MB, MO and RhB solutions with a concentration of 15 mg/L were selected as organic pollutants to further evaluate the photocatalytic activity of HC/BiOCl/BiOBr. It can be seen from the Fig. 6 (c) that HC/BiOCl/BiOBr has strong adsorbability to MB, and the degradation efficiency of 15 mg/L MB by the composite photocatalyst reaches 100% after 30 min of illumination. After 30 min of illumination, the removal rates of RhB and MO by HC/BiOCl/BiOBr composite photocatalyst were 99.41% and 35.38%, respectively. As can be seen from Fig. 6 (d), HC/BiOCl/

BiOBr show better photocatalytic degradation ability under sunlight compared with 7 W LED or 70 W metal halide lamp. After 20 min of sunlight, the degradation efficiency of RhB reached 98.72%.

The reusability of HC/BiOCl/BiOBr was evaluated by repeated degradation of 15 mg/L RhB. As shown in Fig. 6 (e), after 4 cycles, the degradation efficiency of RhB by HC/BiOCl/BiOBr decreased from 99.41 to 83.69%. The degradation efficiency remained above 80%, indicating that the HC/BiOCl/BiOBr had good cycle stability. As can be seen in Fig. 6 (f), there is no significant change in the position and intensity of diffraction peaks of the XRD pattern before and after cycling, indicating that the synthesized HC/BiOCl/BiOBr has good stability.

In order to determine the extent of dye mineralization, chemical oxygen demand (COD) analysis is performed. The lower the COD value, the more inorganic small molecules are generated during the photocatalytic reaction, and the more thoroughly the photocatalytic reaction is carried out. Table 1 shows the mineralization degree of RhB. After 10 min, 20 min and 30 min of irradiation with 70 W gold halide lamp, the COD value of RhB solution is 269.2, 168.5 and 104.8 mg/L, respectively. After 30 min of light exposure, about 78.86% of the dye was mineralized into inorganic small molecules, which further indicated that the sample had good photocatalytic activity.

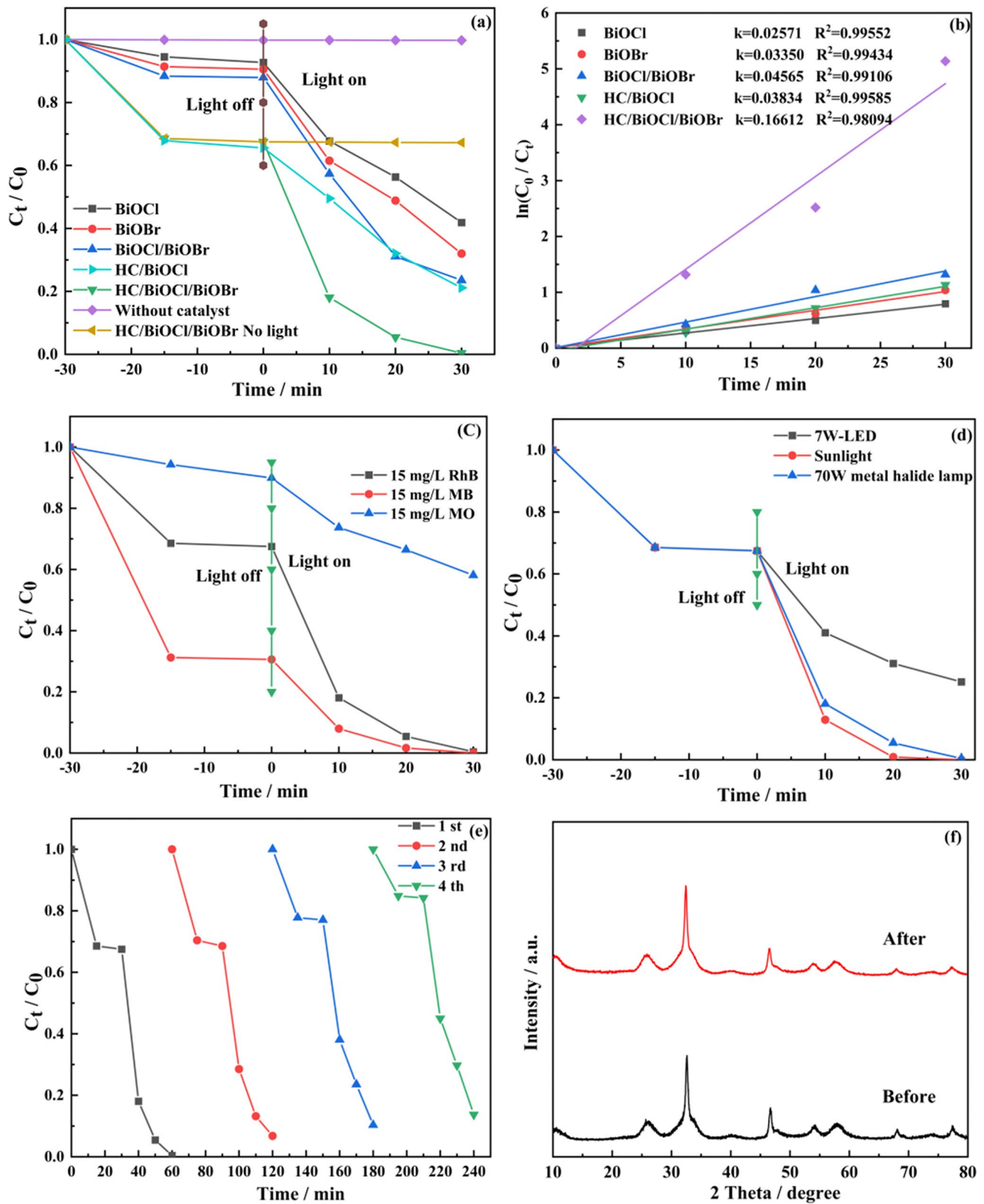


Fig. 6 Degradation curves of different catalyst (a), kinetic curves (b), different dyes (c), under different light sources (d), recycle experiments (e) and XRD diagrams of HC/BiOCl/BiOBr before and after degradation (f)

Table 1 Mineralization degree of RhB

Time	COD	Efficiency
0	495.8	0%
10 min	269.2	45.70%
20 min	168.5	66.01%
30 min	104.8	78.86%

3.3 Analysis of photocatalytic mechanism

The BET surface area and pore size distribution of BiOCl, BiOBr, BiOCl/BiOBr and HC/BiOCl/BiOBr photocatalysts were characterized by nitrogen adsorption-desorption experiments. It can be seen from Fig. 7 that all the samples synthesized are type IV isotherms [26, 27]. Table 2 shows that the average pore sizes of BiOCl, BiOBr, BiOCl/BiOBr and HC/BiOCl/BiOBr composite are 20.53, 29.24, 27.89 and 38.95 nm, respectively. Their specific surface area values were 18.55, 17.67, 14.61 and 17.03 m²/g, respectively.

Table 2 Specific surface areas of the samples

Sample	Specific surface area (m ² /g)	Pore volume (cm ³ /g)	The average pore diameter (nm)
BiOCl	18.55	0.32005	20.53
BiOBr	17.67	0.3796	29.24
BiOCl/BiOBr	14.61	0.2874	27.89
HC/BiOCl/BiOBr	17.03	0.3636	38.95

In order to clearly illustrate the efficient separation and transfer of charge in HC/BiOCl/BiOBr composites, PL and EIS tests were performed. Fig 8 (a) shows the PL spectra of the samples. The results show that pure BiOCl has the highest PL intensity, and the PL intensity decreases significantly after combining with BiOBr and biochar, indicating that HC/BiOCl/BiOBr effectively inhibits the recombination of photogenerated electron-hole. The Electrochemical impedance spectroscopy (EIS) result further proved the

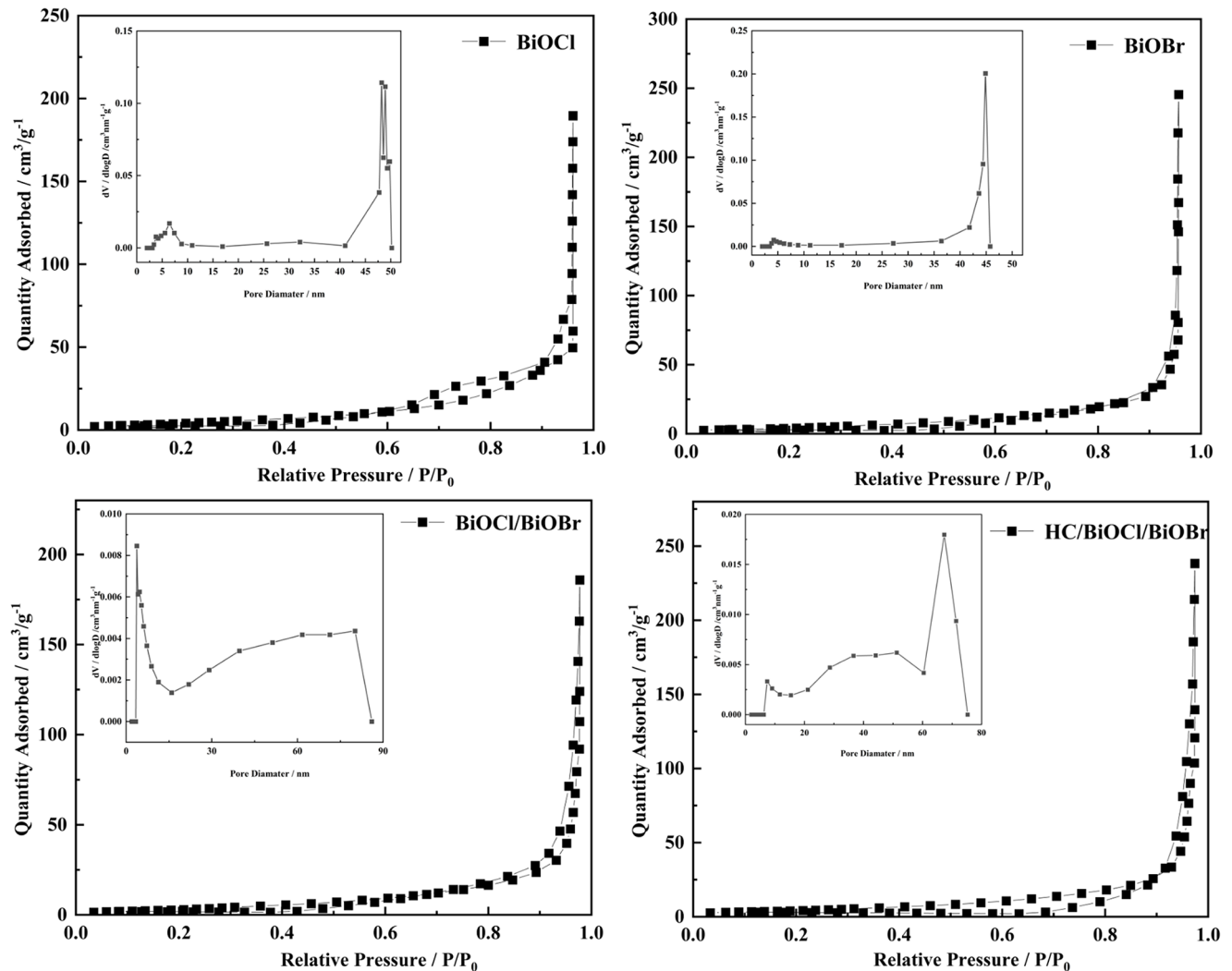


Fig. 7 N₂ adsorption-desorption isotherms and pore size distributions of BiOCl (a), BiOBr (b), BiOCl/BiOBr (c) and HC/BiOCl/BiOBr (d)

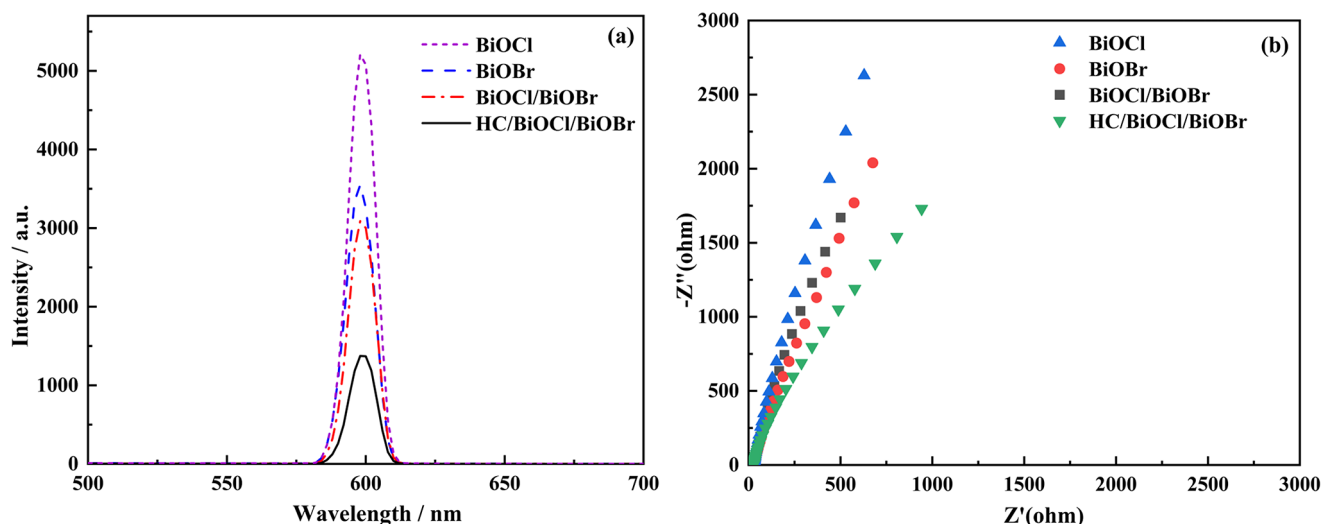


Fig. 8 Photoluminescence diagram (a) and electrochemical impedance diagram (b) of the samples

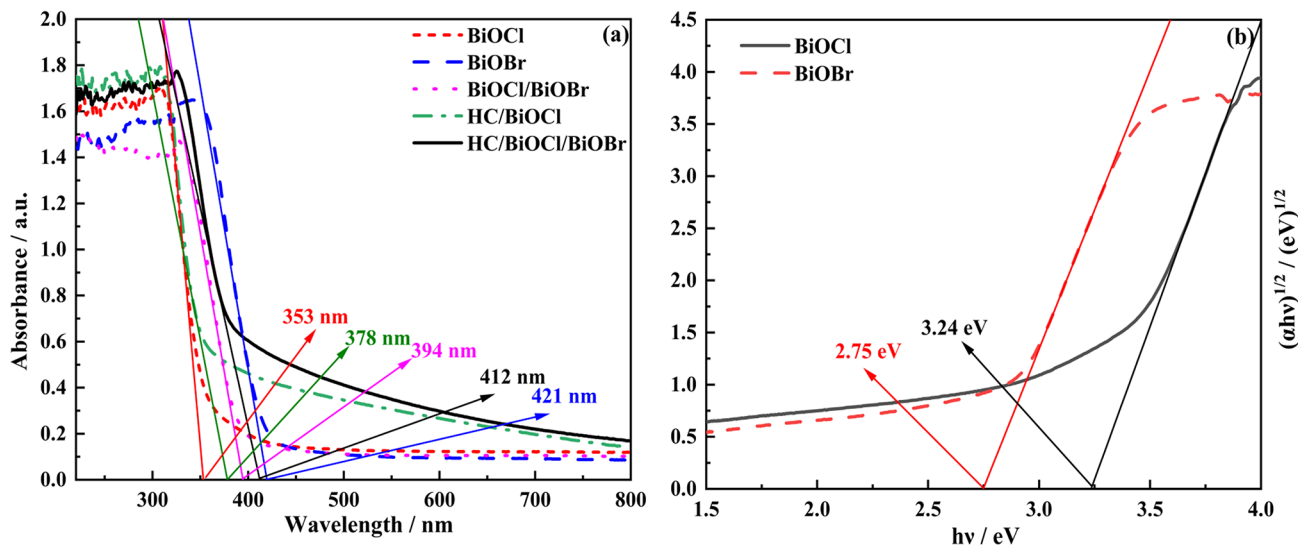


Fig. 9 UV-Vis diffuse reflectance spectra of samples (a), Plot of $(\alpha h\nu)^{1/n}$ versus $h\nu$ (b)

separation efficiency of photoexcited charges. Generally speaking, the smaller the radius of the EIS arc, the higher the charge mobility [28, 29]. As shown in Fig. 8 (b), the arc radius of the EIS Nyquist diagram of HC/BiOCl/BiOBr composite is the smallest, indicating that HC/BiOCl/BiOBr had the lowest electron transfer resistance, thus accelerating the separation and transfer rate of photogenerated carriers. In summary, HC/BiOCl/BiOBr has high carrier separation rate and low recombination rate, so it has good photocatalytic activity.

It is well known that light absorption capacity is very important for the activity of photocatalysts, so it is a key factor in evaluating their catalytic potential [30]. Therefore, a UV-Vis DRS test was performed to determine the light absorption range of the catalyst. As shown in Fig. 9 (a), the light absorption band edge of pure BiOCl is relatively low,

about 353 nm. After the introduction of BiOBr, the absorption edge of HC/BiOCl/BiOBr shows an obvious redshift compared with BiOCl and HC/BiOCl, and the absorption intensity of visible light increases, which may be one of the main reasons for the improvement of its photocatalytic ability. Based on the Tauc equation $(\alpha h\nu)^{1/n} = A(h\nu - E_g)$ (Where E_g , h , A , α and ν represented band gap energy, Planck's constant, constant, optical absorption coefficient and light frequency). BiOCl and BiOBr belongs to the indirect band gap semiconductor and the n value is 2 [31, 32]. According to Fig. 9 (b), the estimated band gap values for BiOCl and BiOBr are 3.24 eV and 2.75 eV, respectively.

TBA, BQ and EDTA-2Na were used as the trapping agents of $\cdot\text{OH}$, $\cdot\text{O}_2^-$ and h^+ , respectively, to reveal the active substances in the photocatalytic degradation process [33]. As shown in Fig. 10, after adding EDTA-2Na, BQ

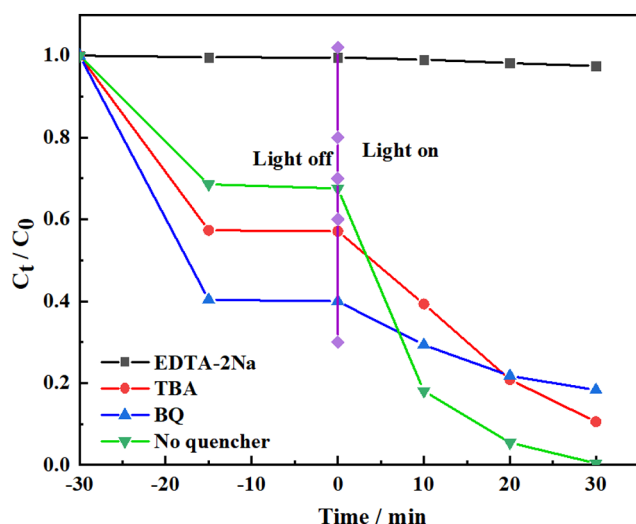


Fig. 10 Trapping experiment of HC/BiOCl/BiOBr

and TBA, the degradation efficiency of RhB by HC/BiOCl/BiOBr composite decreased to 2.1%, 54.19% and 81.5%, respectively, after 30 min irradiation with 70 W gold halide lamp. Therefore, h^+ is the main active species, while $\cdot O_2^-$ plays a secondary role, and $\cdot OH$ has no obvious role.

Combined with the above experimental results, the possible carrier transfer mechanism was deduced, as shown in Fig. 11. The valence band potential (E_{VB}) and conduction band potential (E_{CB}) of semiconductors can be estimated according to formulas $E_{VB} = X - Ee + 0.5 Eg$ and $E_{CB} = E_{VB} - Eg$. According to UV-Vis DRS, the bandgaps of BiOCl and

BiOBr are 3.24 and 2.75 eV respectively. The E_{VB} values of BiOCl and BiOBr are estimated at 2.27 eV and 1.85 eV, and the E_{CB} values are estimated at -0.97 eV and -0.90 eV. When the composite is illuminated by light, e^- in VB is excited and transitions into CB, leaving a relatively stable h^+ in VB. According to the band positions of BiOCl and BiOBr, type I heterojunction may be formed between them. Since the E_{CB} of BiOCl is more negative than that of BiOBr, e^- is transferred from CB of BiOCl to CB of BiOBr, which inhibits the recombination of electron-hole pairs. The effective separation of photogenerated electrons and holes is realized, and the photocatalytic performance of the composite is improved.

4 Conclusions

In summary, HC/BiOCl/BiOBr composites were synthesized by solvothermal method. The results of SEM and TEM showed that HC/BiOCl/BiOBr were assembled from sheet structures into microspheres. Due to its higher charge transfer and visible light absorption capacity, it has higher photocatalytic performance than pure BiOCl. After 30 min irradiation by 70 W metal halide lamp, the degradation efficiency of 15 mg/L RhB by HC/BiOCl/BiOBr was 99.41%, which was 6.46 times and 4.96 times of BiOCl and BiOBr, respectively. EIS and UV-Vis DRS experiments show that the good photocatalytic activity of HC/BiOCl/BiOBr is related to its higher electron-hole pair separation rate and

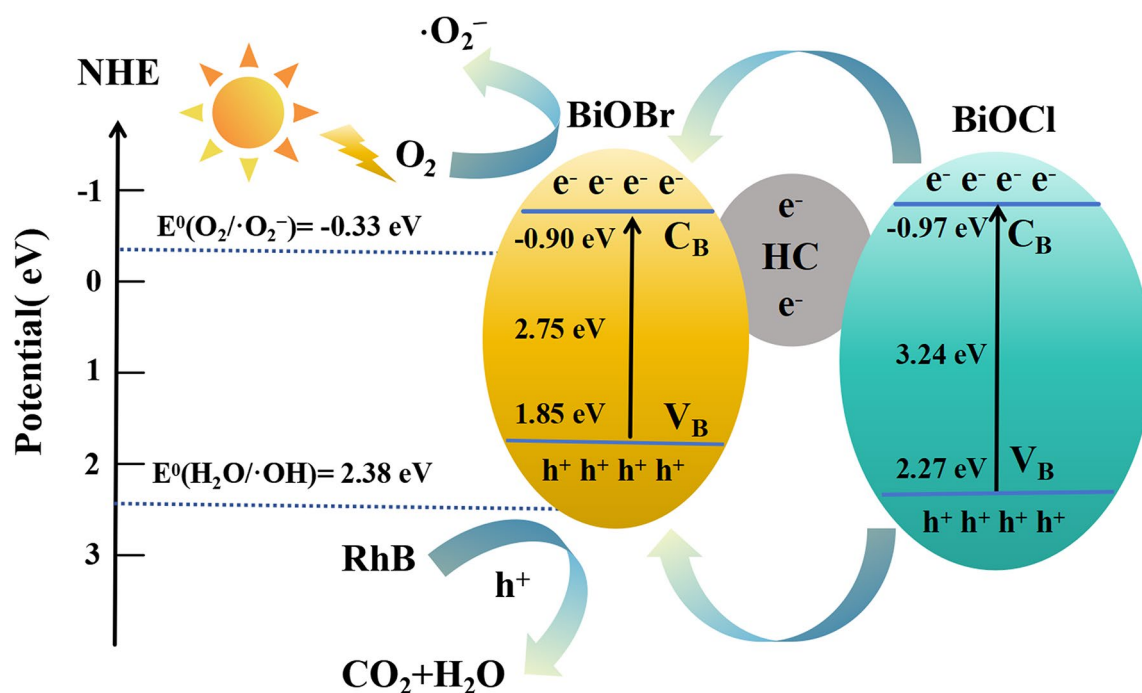


Fig. 11 The photocatalytic mechanism of HC/BiOCl/BiOBr

wider visible light absorption range. The free radical trapping experiment determined that h^+ was the main active species in the photocatalytic reaction, and $\cdot O_2^-$ played a secondary role. In conclusion, the HC/BiOCl/BiOBr can effectively degrade organic pollutants under visible light irradiation.

Acknowledgements This work was financially supported by Project of Heilongjiang Education Department (No. 1453QN023), the Scientific Research Project of Mudanjiang Normal University (No. MNUQN202303).

Authors contributions All authors contributed to the study conception and design. The material preparation, data analysis and writing were done by Xinyu Liu and Yulan Ren. All authors read and approved the final manuscript.

Data availability Data of this study are available from the corresponding author on reasonable request.

Declarations

Conflict of interest The authors declare that they have no conflicts of interest.

References

1. Y.L. Cui, J. Zheng, Z.J. Zhu, C.Y. Hu, B.Z. Liu, Preparation and application of $Bi_4O_7/Cu-BiOCl$ heterojunction photocatalyst for photocatalytic degradation of tetracycline under visible light. *J. Mol. Struct.* **1274**, 134486 (2023)
2. V. Perumal, R. Uthrakumar, M. Chinnathambi, C. Inmozhi, Electron-hole recombination effect of SnO_2-CuO nanocomposite for improving methylene blue photocatalytic activity in wastewater treatment under visible light. *J. King Saud Univ. Sci.* **35**, 102388 (2023)
3. L. Anju Chanu, K. Jugeshwar Singh, K. Nomita Devi, UV light illuminated photodegradation of Malachite green dye using ZnO/CuO nanocomposites. *Materials Today: Proceedings.* **65**, 2865–2870 (2022)
4. J. You, L.Y. Zhang, L.H. He, B.Q. Zhang, Photocatalytic degradation of methyl orange on $ZnO-TiO_2/SO_4^{2-}$ heterojunction composites. *Opt. Mater.* **131**, 112737 (2022)
5. J.L. Wang, K. Wang, Z.H. He, R.G. Zhang, P. Guo, W.T. Wang, Y. Yang, Z.T. Liu, Constructing of ultrathin $Bi_2WO_6/BiOCl$ nanosheets with oxygen vacancies for photocatalytic oxidation of cyclohexane with air in solvent-free. *Appl. Surf. Sci.* **584**, 152606 (2022)
6. S.H. Cen, X.G. Lv, Q.W. Liu, D.Y. Li, Y.L. Jiang, C.X. Hou, P. Zhang, Y. Xu, Direct Z-scheme $Ag_2WO_4/BiOCl$ composite photocatalyst for efficient photocatalytic degradations of dissolved organic impurities. *Optik.* **243**, 166847 (2021)
7. Y. Xu, Z.Z. Li, F. Fang, Y.F. E, G.J. Zhao, Novel visible-light-induced $BiOCl/g-C_3N_4$ photocatalyst for efficient degradation of metronidazole. *Inorg. Chem. Commun.* **132**, 108820 (2021)
8. J. Xu, W. Meng, Y. Zhang, L. Li, C.S. Guo, Photocatalytic degradation of tetrabromobisphenol A by mesoporous BiOBr: efficacy, products and pathway. *Appl. Catal. B* **107**, 355–362 (2011)
9. D. Liu, W.Q. Yao, J. Wang, Y.F. Liu, M. Zhang, Y.F. Zhu, Enhanced visible light photocatalytic performance of a novel heterostructured $Bi_4O_5Br_2/Bi_{24}O_{31}Br_{10}/Bi_2SiO_5$ photocatalyst. *Appl. Catal. B* **172**, 100–107 (2015)
10. X.J. Zou, Y.Y. Dong, X.D. Zhang, Y.B. Cui, X.X. Ou, X.H. Qi, The highly enhanced visible light photocatalytic degradation of gaseous o-dichlorobenzene through fabricating like-flowers $BiPO_4/BiOBr$ p-n heterojunction composites. *Appl. Surf. Sci.* **391**, 525–534 (2017)
11. X.Y. Liu, H.R. Li, S. Gao, X. Jing, Y.L. Ren, Preparation and photocatalytic activity of HC/BiOBr/ Bi_2WO_6 microspheres. *Inorg. Chem. Commun.* **142**, 109695 (2022)
12. Z.Y. Ma, Y.Q. He, X.B. Li, C.H. Zhou, L.J. Deng, Ultrasonic-assisted efficient degradation of tetracycline over $ZnO/BiOBr$ heterojunctions: synergistic effect and role of oxidative species. *Mater. Res. Bull.* **146**, 111591 (2022)
13. L.S. Tan, Z.H. Ma, K.Q. Yang, Q.L. Cui, K. Wang, T.T. Wang, G.L. Wu, J.Y. Zheng, Effect of three artificial aging techniques on physicochemical properties and pb adsorption capacities of different biochars. *Sci. Total Environ.* **699**, 134223 (2020)
14. H.R. Dong, J.M. Deng, Y.K. Xie, C. Zhang, Z. Jiang, Y.Z. Cheng, K.J. Hou, G.M. Zeng, Stabilization of nanoscale zero-valent iron (nZVI) with modified biochar for $Cr(VI)$ removal from aqueous solution. *J. Hazard. Mater.* **332**, 79–86 (2017)
15. J.R. Fan, M.J. Bai, H.R. Zhang, Y.Y. Chu, Synthesis and immobilization of HC/ $BiVO_4$ catalyst particles with PTFE for photocatalytic tetracycline degradation: Preparation, performance and mechanism. *J. Water Process. Eng.* **56**, 104474 (2023)
16. Y.L. Ren, Y.W. Zhu, S. Gao, X.Y. Liu, H.R. Li, S.P. Rui, Preparation of HC/BiOCl composite photocatalyst and its visible photocatalytic performance. *Inorg. Chem. Commun.* **163**, 112329 (2024)
17. Y. He, Y.F. Wang, J. Hu, K.J. Wang, Y.W. Zhai, Y.Z. Chen, Y.B. Duan, Y.T. Wang, W.J. Zhang, Photocatalytic property correlated with microstructural evolution of the biochar/ZnO composites. *J. Mater. Res. Technol.* **11**, 1308–1321 (2021)
18. Y.F. Wu, M.J. Xu, Y.Q. Wang, B. Hu, Y. Xie, Y. Ling, BiOCl/BiOBr composites for efficient photocatalytic carbon dioxide reduction. *Appl. Catal. A-Gen.* **677**, 119708 (2024)
19. A.B. Wang, L.J. Xu, L. Gan, C.T. Mei, L.J. Wang, X.Y. Fang, M.R. Li, M.Z. Pan, S.G. Han, J.Q. Cui, Using wood flour waste to produce biochar as the support to enhance the visible-light photocatalytic performance of BiOBr for organic and inorganic contaminants removal. *Chemosphere.* **250**, 126291 (2020)
20. Q.Y. Zhang, Z.X. Yang, R. Zhang, Y. Hao, L.J. Xu, C.L. Liu, A novel recyclable $BiOCl/BiOI/Mn_xZn_{1-x}Fe_2O_4$ photocatalyst with enhanced rhodamine B removal under visible light. *J. Phys. Chem. Solids.* **170**, 110892 (2022)
21. Y.X. Yin, Y. Yao, X.Y. Qian, M.F. Sun, B.J. Huang, G.Y. He, H.Q. Chen, Fabrication of $Fe/BiOCl/RGO$ with enhanced photocatalytic degradation of ciprofloxacin under visible light irradiation. *Mater. Sci. Semicond. Process.* **140**, 106384 (2022)
22. T. Zhang, M. Maihemllti, K. Okitsu, D. Talifur, Y. Tursun, A. Abulizi, In situ self-assembled S-scheme BiOBr/pCN hybrid with enhanced photocatalytic activity for organic pollutant degradation and CO_2 reduction. *Appl. Surf. Sci.* **556**, 149828 (2021)
23. Z.B. Liu, X.J. Yu, P.H. Gao, J.K. Nie, F. Yang, B.Q. Guo, J. Zhang, Preparation of $BiOCl/Cu_2O$ composite particles and its photocatalytic degradation of moxifloxacin. *Opt. Mater.* **128**, 112432 (2022)
24. L. Guo, Y. You, H.W. Huang, N. Tian, T.Y. Ma, Y.H. Zhang, Z-scheme $g-C_3N_4/Bi_2O_2[BO_2(OH)]$ heterojunction for enhanced photocatalytic CO_2 reduction. *J. Colloid Interface Sci.* **568**, 139–147 (2020)
25. Z. Li, M. Li, Z.Y. Wang, X. Liu, Coadsorption of $Cu(II)$ and tylosin/sulfamethoxazole on biochar stabilized by nano-hydroxyapatite in aqueous environment. *Chem. Eng. J.* **381**, 122785 (2020)

26. X.F. Qu, M.H. Liu, L.F. Li, R. Wang, H. Sun, L. Shi, F.L. Du, BiOBr flakes decoration and structural modification for CdTe/TiO₂ spheres: towards water decontamination under simulated light irradiation. *Mater. Sci. Semicond. Process.* **93**, 331–338 (2019)
27. Z.Y. Yang, L. Chen, Y. Yang, J.J. Wang, Y.K. Huang, X.X. Liu, S.J. Yang, Constructing TiO₂ decorated Bi₂WO₆ architectures with enhanced visible-light-driven photocatalytic activity. *Semicond. Sci. Technol.* **32**, 065008 (2017)
28. M. Li, H.W. Huang, S.X. Yu, N. Tian, F. Dong, X. Du, Y.H. Zhang, Simultaneously promoting charge separation and photoabsorption of BiOX (X = cl, br) for efficient visible-light photocatalysis and photosensitization by compositing low-cost biochar. *Appl. Surf. Sci.* **386**, 285–295 (2016)
29. R.Y. Wu, H.B. Song, N. Luo, G.J. Ji, Hydrothermal preparation of 3D flower-like BiPO₄/Bi₂WO₆ microsphere with enhanced visible-light photocatalytic activity. *J. Colloid Interface Sci.* **524**, 350–359 (2018)
30. X.D. Tang, Z.R. Wang, N. Wu, S.L. Liu, N. Liu, A novel visible-light-active β-Bi₂O₃/BiOBr heterojunction photocatalyst with remarkably enhanced photocatalytic activity. *Catal. Commun.* **119**, 119–123 (2019)
31. Q.H. Zhao, X.Y. Liu, Y.X. Xing, Z.L. Liu, C.F. Du, Synthesizing Bi₂O₃/BiOCl heterojunctions by partial conversion of BiOCl. *J. Mater. Sci.* **52**, 2117–2130 (2017)
32. S. Fu, X.M. Liu, Y.H. Yan, L. Li, H.P. Liu, F.Y. Zhao, J.G. Zhou, Few-layer WS₂ modified BiOBr nanosheets with enhanced broad-spectrum photocatalytic activity towards various pollutants removal. *Sci. Total Environ.* **694**, 133756 (2019)
33. N. Wang, L. Shi, L.Z. Yao, C.Y. Lu, Y. Shi, J.M. Sun, Highly improved visible-light-induced photocatalytic performance over BiOI/Ag₂CO₃ heterojunctions. *RSC Adv.* **8**, 537–546 (2018)

Publisher's note Springer Nature remains neutral with regard to jurisdictional claims in published maps and institutional affiliations.

Springer Nature or its licensor (e.g. a society or other partner) holds exclusive rights to this article under a publishing agreement with the author(s) or other rightsholder(s); author self-archiving of the accepted manuscript version of this article is solely governed by the terms of such publishing agreement and applicable law.